J|A|C|S
ARTICLES
Published on Web 08/24/2004

Phototriggered Self-Assembly of Hydrogen-Bonded Rosette

Shiki Yagai,*,† Toshiharu Nakajima,† Takashi Karatsu,† Ken-ichi Saitow,‡ and Akihide Kitamura†

Contribution from the Department of Materials Technology, Faculty of Engineering, and Department of Physics, Faculty of Science, Chiba University, 1-33 Yayoi-cho, Inage-ku, Chiba 263-8522, Japan

Received April 17, 2004; E-mail: yagai@faculty.chiba-u.jp

Abstract: Azobenzene-appended melamine **M2** and barbiturate **B2**, both possessing bulky tridodecyloxyphenyl (TDP) wedge(s), were designed and synthesized to establish a photoresponsive hydrogen-bonded supramolecular assembly. The geometrical isomer *EE*-**M2** bearing two *E*-azobenzene moieties easily complexed with **B2**, affording a remarkably stable cyclic hexamer *EE*-**M2**$_3$·**B2**$_3$ (rosette) in chloroform, toluene, and methylcyclohexane, as confirmed by size exclusion chromatography, dynamic light scattering, ^{1}H NMR, and UV−vis studies. The $E \rightarrow Z$ photoisomerization of the azobenzene moieties upon irradiation with UV light was significantly suppressed in the rosette because of the steric crowding of the TDP wedges (total of nine TDP wedges in a rosette), whereas irradiation of the monomeric *EE*-**M2** resulted in facile transformation into *ZZ*-**M2** bearing two *Z*-azobenzene moieties. ^{1}H NMR studies of the complexation of the initially photogenerated *ZZ*-**M2** with **B2** revealed that it is hard for *ZZ*-**M2** to form a rosette with **B2** because of the intermolecular steric interaction between the TDP wedges. The photoregulatable complexation efficiency of **M2** allowed us to accomplish the phototriggered formation of the rosette by irradiation of a monomeric mixture of *ZZ*-**M2** and **B2** using visible light.

Introduction

The manipulation of self-assembling small molecules into nanoscale objects by external inputs realizes the creation of stimuli-responsive smart nanomaterials with functions that can be output at any time on demand. A particularly promising approach in this interesting field is the use of the photoisomerization reaction of photochromic molecules. Nature uses this principle in vision as the most prominent example.[1] A variety of photoresponsive molecules has been utilized as photoswitching units to control the structure and the function of supramolecular systems.[1a,2] Azobenzene has been especially incorporated into diverse kinds of supramolecules,[3−9] since its *E*/*Z* isomerization is accompanied by the large changes in molecular geometry, advantageous for inducing dramatic structural changes in the systems.

The flat structure of *E*-azobenzene is apt to undergo $\pi-\pi$ stacking, favorable for creating a polymeric assembly. On the contrary, the folded structure of *Z*-azobenzene is generally unfavorable for stacking.[10] This structural difference accompanying isomerization has been successfully utilized to create photoresponsive "extended assemblies" as seen in many examples of the azobenzene-incorporated membranous systems.[4] Creation of a photoresponsive discrete self-assembly with a well-defined shape is, however, challenging because of the difficulty

† Department of Materials Technology, Faculty of Engineering.
‡ Department of Physics, Faculty of Science.

(1) (a) Dugave, C.; Demange. L. *Chem. Rev.* **2003**, *103*, 2475−2532. (b) Bohran, B.; Souto, M. L.; Imai, H.; Shichida, Y.; Nakanishi, K. *Science* **2000**, *288*, 2209−2212. (c) Wald, G. *Science* **1968**, *162*, 230−239.
(2) Feringa, B. L.; van Delden, R. A.; Koumura, N.; Geertsema, E. M. *Chem. Rev.* **2000**, *100*, 1789−1816.
(3) For examples of azobenzene-incorporated purely organic and biomolecular self-assemblies, see: (a) Rakotondradany, F.; Whitehead, M. A.; Lebuis, A.-M.; Sleiman, H. F. *Chem.−Eur. J.* **2003**, *9*, 4771−4780. (b) Liu, N.; Yu, K.; Smarsly, B.; Dunphy, D. R.; Jiang, Y.-B.; Brinker, C. J. *J. Am. Chem. Soc.* **2002**, *124*, 14540−14541. (c) Liang, X.; Asanuma, H.; Komiyama, M. *J. Am. Chem. Soc.* **2002**, *124*, 1877−1883. (d) Sun, S.-S.; Anspach, J. A.; Lees, A. J. *Inorg. Chem.* **2002**, *41*, 1862−1869. (e) Asanuma, H.; Ito, T.; Yoshida, T.; Liang, X.; Komiyama, M. *Angew. Chem., Int. Ed.* **1999**, *38*, 2393−2395. (f) Asakawa, M.; Ashton, P. R.; Balzani, V.; Brown, C. L.; Credi, A.; Matthews, O. A.; Newton, S. P.; Raymo, F. M.; Shipway, A. N.; Spender, N.; Quick, A.; Stoddart, J. F.; White, A. J. P.; Williams, D. J. *Chem.−Eur. J.* **1999**, *5*, 860−875. (g) Vollmer, M. S.; Clark, T. D.; Steinem, C.; Ghadiri, M. R. *Angew. Chem., Int. Ed.* **1999**, *38*, 1598−1601. (h) Murata, K.; Aoki, M.; Nishi, T.; Ikeda, A.; Shinkai, S. *J. Chem. Soc., Chem. Commun.* **1991**, 1715−1718.
(4) For examples of azobenzene-incorporated lipids, vesicles, micelles, and bilayers, see: (a) Kuiper, J. M.; Engberts, J. B. F. N. *Langmuir* **2004**, *20*, 1152−1160. (b) Kawasaki, T.; Tokuhiro, M.; Kimizuka, N.; Kunitake, T. *J. Am. Chem. Soc.* **2001**, *123*, 6792−6800. (c) Orihara, Y.; Matsumura, A.; Saito, Y.; Ogawa, N.; Saji, T.; Yamaguchi, A.; Sakai, H.; Abe, M. *Langmuir* **2001**, *17*, 6072−6076. (d) Einaga, Y.; Sato, O.; Iyoda, T.; Fujishima, A.; Hashimoto, K. *J. Am. Chem. Soc.* **1999**, *121*, 3745−3750. (e) Song, X.; Perlstein, J.; Whitten, D. G. *J. Am. Chem. Soc.* **1997**, *119*, 9144−9159. (f) Shimomura, M.; Kunitake, T. *J. Am. Chem. Soc.* **1987**, *109*, 5175−5183. (g) Kunitake, T.; Nakashima, N.; Shimomura, M.; Okahara, Y. *J. Am. Chem. Soc.* **1980**, *102*, 6644−6646.
(5) For examples of azobenzene-incorporated liquid crystalline materials, see: (a) Ichimura, K. *Chem. Rev.* **2000**, *100*, 1847−1873. (b) Moriyama, M.; Mizoshita, N.; Yokota, T.; Kishimoto, K.; Kato, T. *Adv. Mater.* **2003**, *15*, 1335−1338. (c) Prasad, S. K.; Nair, G. G. *Adv. Mater.* **2001**, *13*, 40−43. (d) Moriyama, M.; Tamaoki, N. *Chem. Lett.* **2001**, 1142−1143.
(6) For examples of azobenzene-incorporated Langmuir−Brodgett films, see: (a) Azumi, R.; Kakiuchi, K.; Matsumoto, M. *Chem. Lett.* **2004**, *33*, 172−173. (b) Seki, T.; Fukuchi, T.; Ichimura, K. *Langmuir* **2002**, *18*, 5462−5467. (c) Patton, D.; Park, M.-K.; Wang, S.; Advincula, R. C. *Langmuir* **2002**, *18*, 1688−1694. (d) Sidorenko, A.; Houphouet-Boigny, C.; Villavicencio, O.; Hashemzadeh, M.; McGrath, D. V.; Tsukruk, V. V. *Langmuir* **2000**, *16*, 10569−10572. (e) Matsumoto, M.; Miyazaki, D.; Tanaka, M.; Azumi, R.; Manda, E.; Kondo, Y.; Yoshino, N.; Tachibana, H. *J. Am. Chem. Soc.* **1998**, *120*, 1479−1484. (f) Tachibana, H.; Nakamura, T.; Matsumoto, M.; Komizu, H.; Manda, E.; Niino, H.; Yabe, A.; Kawabata, Y. *J. Am. Chem. Soc.* **1989**, *111*, 3080−3081.

10.1021/ja047783z CCC: $27.50

Chart 1. Supramolecular Synthons

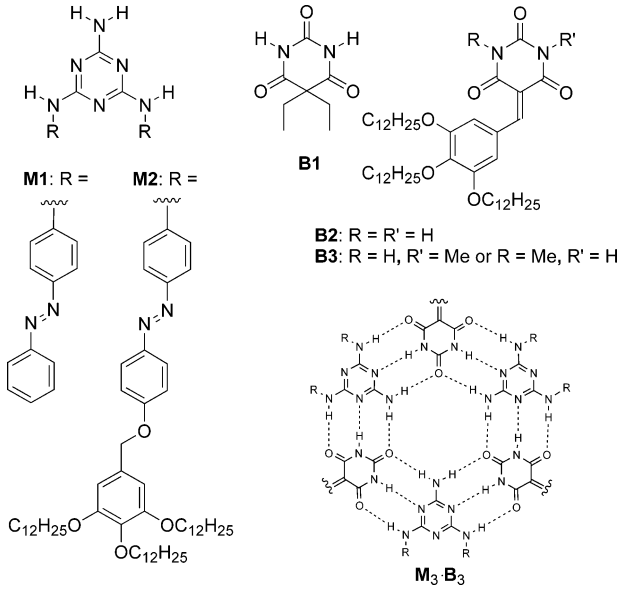

in applying the geometrical changes of azobenzene to such discrete self-assembling systems. Here, we present a notable example of the photoresponsive discrete self-assembly using a hydrogen-bond directed cyclic hexamer (rosette) formed between melamine and barbituric acid.[11]

Recently, we reported a photoresponsive rosette composed of azobenzene-containing melamine **M1** and barbiturate **B1**

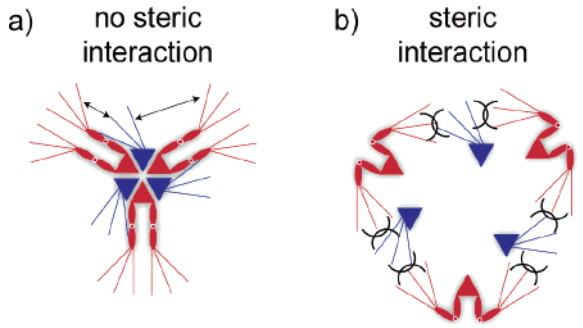

Figure 1. Schematic representation of the aggregation between **M2** (red) and **B2** (blue) when the two azobenzene moieties of **M2** take (a) *E*- or (b) *Z*-conformations. For **M2**, the *E*- and *Z*-conformations of the azobenzene moieties are shown by folding their arms.

(Chart 1).[12] In this system, the $E \rightarrow Z$ isomerization of the azobenzene moieties in rosette $\mathbf{M1}_3 \cdot \mathbf{B1}_3$ formed in $CDCl_3$ indirectly stabilized the rosette by increasing the solubilities of the competing oligomeric tapelike assemblies. As an extension of this work, in the present study **M2** and **B2** are designed to realize a more direct photochemical control in their self-assembling process (Chart 1). Melamine **M2** and barbiturate **B2** are modulated by introducing tri(dodecyloxy)phenyl (TDP) wedge(s). As schematically shown in Figure 1a, when the azobenzene moieties of **M2** take the *E*-conformations, the bulky TDP wedges stabilize the rosette by covering the hydrogen-bonding core. In contrast, when the two azobenzene moieties of **M2** take the *Z*-conformation (Figure 1b), the TDP wedges sterically interfere with the formation of the rosette.[13] On the basis of the photoinduced structural transformation of **M2**, the formation of the stable discrete cyclic assemblies $\mathbf{M2}_3 \cdot \mathbf{B2}_3$ was controlled by light.

Experimental Section

General. The synthesis of azobenzene-appended **M2** and barbiturates **B2** and **B3** are detailed in the Supporting Information. Tetrahydrofuran was distilled over sodium/benzophenone. Column chromatography was performed on 63−210 μm silica gel. Solvents used for the measurements were all spectral grade and used without further purification. All other commercially available reagents and solvents were of reagent grade and used without further purification.

1D and 2D ^{1}H NMR (400 MHz) spectra were recorded on a JEOL LA400 spectrometer. Chemical shifts are reported in parts per million with the signal of the residual solvent ($CHCl_3$) as the internal standard. IR spectra were recorded on a JASCO FT/IR-410. UV spectra were measured on a JASCO V570 spectrophotometer. FAB-MS spectra were measured on a JEOL JMS-AX500 mass spectrometer. Elemental analyses were performed at Analytical Center of Chiba University.

Size Exclusion Chromatography. Analytical size exclusion chromatography (SEC) was performed on the system composed of a Hitachi 655 HPLC, Hitachi UVIDEC-100-II UV detector, and Waters gel permeation column (Ultrastyragel, 1000 Å pore size). All measurements were conducted at 20 °C. HPLC-grade toluene was used as the eluent. The flow rate was 1 mL/min. The detection wavelength was set to 325 nm.

Dynamic Light Scattering Studies. Dynamic light scattering measurements were performed with an Ar laser operating at 514.5 nm with 300 mW laser power. Details of the instruments are available

(7) For examples of azobenzene-based molecular machines, see: (a) Muraoka, T.; Kinbara, K.; Kobayashi, Y.; Aida, T. *J. Am. Chem. Soc.* **2003**, *125*, 5612−5613. (b) Jeong, K.-S.; Chang, K.-J.; An, Y.-J. *Chem. Commun.* **2003**, 1450−1451. (c) Stanier, C. A.; Alderman, S. J.; Claridge, T. D. W.; Anderson, H. L. *Angew. Chem., Int. Ed.* **2002**, *41*, 1769−1772. (d) Willner, I.; Pardo-Yissar, V.; Katz, E.; Ranjit, K. T. *J. Electroanal. Chem.* **2001**, *497*, 172−177. (e) Harada, A. *Acc. Chem. Res.* **2001**, *34*, 456−464. (f) Asakawa, M.; Ashton, P. R.; Balzani, V.; Brown, C. L.; Credi, A.; Matthews, O. A.; Newton, S. P.; Raymo, F. M.; Shipway, A. N.; Spender, N.; Quick, A.; Stoddart, J. F.; White, A. J. P.; Williams, D. J. *Chem.−Eur. J.* **1999**, *5*, 860−875. (g) Murakami, H.; Kawabuchi, A.; Kotoo, K.; Kunitake, M.; Nakashima, N. *J. Am. Chem. Soc.* **1997**, *119*, 7605−7606.
(8) For examples of an azobenzene-incorporated host−guest complex, see: (a) Otsuki, J.; Narutaki, K.; Bakke, J. M. *Chem. Lett.* **2004**, *33*, 356−357. (b) Hunter, C. A.; Togrul, M.; Tomas, S. *Chem. Commun.* **2004**, 108−109. (c) Banerjee, I. A.; Yu, L.; Matsui, H. *J. Am. Chem. Soc.* **2003**, *125*, 9542−9543. (d) Cacciapaglia, R.; Stefano, S. D.; Mandolini, L. *J. Am. Chem. Soc.* **2003**, *125*, 2224−2227. (e) Srinivas, O.; Mitra, N.; Surolia, A.; Jayaraman, N. *J. Am. Chem. Soc.* **2002**, *124*, 2124−2125. (f) Goodman, A.; Breinlinger, E.; Ober, M.; Rotello, V. M. *J. Am. Chem. Soc.* **2001**, *123*, 6213−6214. (g) Shinmori, H.; Takeuchi, M.; Shinkai, S. *J. Chem. Soc., Perkin Trans. 2* **1998**, 847−852. (h) Würthner, F.; Rebek, J., Jr. *Angew. Chem., Int. Ed. Engl.* **1995**, *34*, 446−448. (i) Würthner, F.; Rebek, J., Jr. *J. Chem. Soc., Perkin Trans. 2* **1995**, 1727−1734. (j) Shinkai, S.; Minami, T.; Kusano, Y.; Manabe, O. *J. Am. Chem. Soc.* **1983**, *105*, 1851−1856. (k) Shinkai, S.; Nakaji, T.; Nishida, Y.; Ogawa, T.; Manabe, O. *J. Am. Chem. Soc.* **1980**, *102*, 5860−5865. (l) Bartels, E.; Wassermann, N. H.; Erlanger, B. F. *Proc. Natl. Acad. Sci. U.S.A.* **1971**, *8*, 1820−1823.
(9) For examples of azobenzene-incorporated dendrimers, see: (a) Liao, L.-X.; Stellacci, F.; McGrath, D. V. *J. Am. Chem. Soc.* **2004**, *126*, 2181−2185. (b) Nithyanandhan, J.; Jayaraman, N.; Davis, R.; Das, S. *Chem.−Eur. J.* **2004**, *10*, 689−698. (c) Weener, J.-W.; Meijer, E. W. *Adv. Mater.* **2000**, *12*, 741−746. (d) Ghosh, S.; Banthia, A. K. *Tetrahedron Lett.* **2001**, *42*, 501−503. (e) Archut, A.; Azzellini, G. C.; Balzani, V.; Cola, L. D.; Vögtle, F. *J. Am. Chem. Soc.* **1998**, *120*, 12187−12191. (f) Junge, D. M.; McGrath, D. V. *J. Am. Chem. Soc.* **1999**, *121*, 4912−4913. (g) Cattani-Scholz, A.; Renner, C.; Oesterhelt, D.; Moroder, L. *ChemBioChem* **2001**, *2*, 542−549. (h) Jiang, D.-J.; Aida, T. *Nature* **1997**, *388*, 454−456.
(10) Recently, Sleiman et al. reported cyclic tetramer of (*Z*)-azodibenzoic acid derivatives that hierarchically grow into a rodlike edifice by $\pi-\pi$ stacking (see ref 3a)
(11) Reviews: (a) Timmerman, P.; Prins, L. J. *Eur. J. Org. Chem.* **2001**, 3191−3205. (b) Sherrington, D. C.; Taskinen, K. A. *Chem. Soc. Rev.* **2001**, *30*, 83−93. (c) Prins, L. J.; Reinhoudt, D. N.; Timmerman, P. *Angew. Chem., Int. Ed.* **2001**, *40*, 2382−2426. (d) Whitesides, G. M.; Simanek, E. E.; Mathias, J. P.; Seto, C. T.; Chin, D. N.; Mammen, M.; Gordon, D. M. *Acc. Chem. Res.* **1995**, *28*, 37−44. (e) Lawrence, D. S.; Jiang, T.; Levett, M. *Chem. Rev.* **1995**, *95*, 2229−2260.
(12) Yagai, S.; Karatsu, T.; Kitamura, A. *Chem. Commun.* **2003**, 1844−1845.
(13) Since each azobenzene moiety of **M2** is capable of *E*/*Z* isomerization, **M2** exists as three discrete isomers: *EE*-**M2**, *EZ*-**M2**, and *ZZ*-**M2**. The two azobenzene moieties of **M2** under daylight conditions exclusively take the *E*-form (*EE*-**M2**, 99% isomeric purity) based on the ^{1}H NMR spectrum.

elsewhere.[14] Sample solutions (1.5×10^{-5} mol of samples in 3 mL of spectral grade chloroform) were all filtered (0.2 μm, Millipore) before measurements and put into cylindrical quartz cuvettes and kept at 10 °C. The scattering angle was set to 40°. During the measurements, dried nitrogen gas was passed around the index matching vat, including the cuvette, to avoid condensation. The data acquisition was performed using multiple-tau digital correlator (ALV5000E). The autocorrelation functions thus obtained were well-characterized double-exponentially (for *EE*-**M2**) or single-exponentially (for *EE*-**M2**$_3$**B2**$_3$) to obtain the diffusion coefficiencies D. The average hydrodynamic radii were calculated from the Storks−Einstein equation ($R_h = k_BT/6\pi\eta D$).

Molecular Modeling Calculations. Molecular modeling calculations were performed on a HYPERCHEM version 5.1 (HYPERCUBE Co.) software package. **M2** and **B2** were independently energy-minimized using MM+ and PM3 calculations.[15] The resulting monomeric components were docked in the rosette motif. The hydrogen-bond distances in the DAD·ADA array were all restricted to 2.1 Å, and the rosette was energy-minimized by MM+ calculations on the basis of Newton Raphson block diagonal algorithm with a stop criterion of gradient <0.01.

NMR Studies. ^{1}H NMR titrations of **M2** (*EE*- or *ZZ*-isomer) with **B2** were performed at 20 °C for 5 mM $CDCl_3$ solution of **M2** with an initial volume of 0.4 mL. Aliquots of a $CDCl_3$ solution containing **B2** (50 mM) and **M2** (5 mM) were added to the solution. After sufficient mixing, the ^{1}H NMR spectrum was recorded. This procedure was repeated. DMSO titration study was carried out using a 5 mM $CDCl_3$ solution of *EE*-**M2**$_3$·**B2**$_3$ (0.6 mL). A volume of 10 μL of DMSO-d_6 was added to the solution. After sufficient mixing, the ^{1}H NMR spectrum was recorded at 20 °C. This procedure was repeated until the aggregates were no longer observed. NMR dilution study was carried out as follows: The ^{1}H NMR spectrum of a 0.6-mL $CDCl_3$ solution of *EE*-**M2**$_3$·**B2**$_3$ (100 mM) was recorded at 20 °C. A 0.3-mL aliquot of the solution was removed, and the 0.3 mL of $CDCl_3$ was added. After sufficient mixing, the ^{1}H NMR spectrum was recorded. This procedure was repeated until the aggregates were no longer observed (<0.05 mM).

UV−Vis Studies. Variable-temperature UV−vis measurements were performed using a 10 μM MCH solution of the *EE*-**M2**$_3$·**B2**$_3$ in a 1-cm quartz cuvette. The UV−vis dilution study was performed at 20 °C in a manner similar to the NMR dilution studies. For the concentrated ($>10^{-4}$ M) and diluted solution ($<10^{-6}$ M), 5-cm and 1-mm cuvettes were used for the measurements, respectively.

Photoirradiation Studies. Photoirradiation was performed using a fluorimeter equipped with a 150 W xenon lamp (20 nm bandwidth) in a quartz cuvette (samples for UV−vis and SEC studies) or 5-mm NMR sample tube (samples for NMR studies).

Phototriggered Self-Assembly Study Using SEC. An equimolar mixture of *ZZ*-**M2** (ca. 94% isomeric purity) and **B2** ([**M2**] = [**B2**] = 50 μM) in toluene (3 mL) was placed in a quartz cuvette. The cuvette was placed in the fluorimeter at 20 °C and irradiated at around 450-nm light for several minutes. After the irradiation was stopped, 50 μL of the solution was analyzed by SEC at 20 °C. Fifteen minutes after the injection of the sample, the UV−vis spectrum of the residual solution was recorded. This procedure was repeated until the SEC peak of the rosette no longer showed any detectable changes (25 min). Because of the relatively slow $Z \rightarrow E$ thermal isomerization at 20 °C ($t_{1/2}$ = 4 h), the time lag between the SEC and UV−vis analyses is almost negligible.

Results and Discussion

Characterization of Rosette. Since the highly directional binding property of the hydrogen bond is particularly useful for obtaining well-defined assemblies, stabilization of the assemblies based on this relatively weak interaction is a challenging subject.[11,16−19] In the present study, the introduction of TDP wedges effectively stabilizes the rosette *EE*-**M2**$_3$·**B2**$_3$ in comparison with the previous rosette *EE*-**M1**$_3$·**B1**$_3$ lacking the TDP wedges. Rosette *EE*-**M2**$_3$·**B2**$_3$ was characterized by SEC, dynamic light scattering (DLS), ^{1}H NMR, and UV−vis studies.[20]

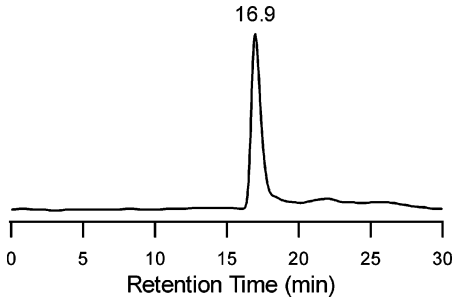

Figure 2. SEC chromatogram of the equimolar mixture of *EE*-**M2** (50 μM) and **B2** (50 μM) in toluene.

Size Exclusion Chromatography Studies. Aggregation between *EE*-**M2** (99% isomeric purity) and **B2** was studied by SEC using toluene as the eluent. The detection of hydrogen-bonded assemblies by SEC requires enough stability to elute from the column without decomposition.[16,18c,21−23] The individual components, *EE*-**M2** and **B2**, scarcely eluted from the column because their polar functionalities strongly interact with the column matrix.[18c,21] In sharp contrast, injection of an equimolar mixture of *EE*-**M2** and **B2** gave a single sharp peak (Figure 2), the retention time (16.9 min) of which is independent of the injection concentration (0.05−5 mM). The polydispersity index of the peak is 1.08, indicating the formation of monodisperse aggregates. These SEC behaviors can be taken as evidence for the formation of a discrete cyclic assembly. The molecular weight determined using polystyrene (PS) standards for calibration is 14 800, which is 1.92-fold larger than the calculated value for *EE*-**M2**$_3$·**B2**$_3$ (MW = 7716). The overes-

(14) Saitow, K.; Ochiai, H.; Kato, T.; Nishikawa, K. *J. Chem. Phys.* **2002**, *116*, 4985−4992.
(15) Yagai, S.; Miyatake, T.; Shimono, Y.; Tamiaki, H. *Photochem. Photobiol.* **2001**, *73*, 153−163.
(16) Ma, Y.; Kolotuchin, S. V.; Zimmerman, S. C. *J. Am. Chem. Soc.* **2002**, *124*, 13757−13769.
(17) Félix, O.; Crego-Calama, M.; Luyten, I.; Timmerman, P.; Reinhoudt, D. N. *Eur. J. Org. Chem.* **2003**, 1463−1474.
(18) Cyclic hexamer based on GC-hybrid molecules: (a) Fenniri, H.; Deng, B.-L.; Ribbe, A. E. *J. Am. Chem. Soc.* **2002**, *124*, 11064−11072. (b) Fenniri, H.; Mathivanan, P.; Vidale, K. L.; Sherman, D. M.; Hallenga, K.; Wood, K. V.; Stowell, J. G. *J. Am. Chem. Soc.* **2001**, *123*, 3854−3855. (c) Kolotuchin, S. V.; Zimmerman, S. C. *J. Am. Chem. Soc.* **1998**, *120*, 9092−9093. (d) Marsh, A.; Silvestri, M.; Lehn, J.-M. *Chem. Commun.* **1996**, 1527−1528. Mascal et al. also reported GC-hybrid molecules that selectively self-assemble into the rosette motif in the solid state: (e) Mascal, M.; Hext, N. M.; Warmuth, R.; Arnall-Culliford, J. R.; Moore, M. H.; Turkenburg, J. P. *J. Am. Chem. Soc.* **1999**, *64*, 8479−8484. (f) Mascal, M.; Hext, N. M.; Warmuth, R.; Moore, M. H.; Turkenburg, J. P. *Angew. Chem., Int. Ed. Engl.* **1996**, *35*, 2204−2206. In these articles, no solution studies were reported.
(19) Hirschberg, J. H. K. K.; Brunsveld, L.; Ramzi, A.; Vekemans, J. A. J. M.; Sijbesma, R. P.; Meijer, E. W. *Nature* **2000**, *407*, 167−170.
(20) Attempts to detect *EE*-**M2**$_3$·**B2**$_3$ in chloroform by electrospray ionization (ESI), coldspray ionization (CSI), and matrix-assisted laser desorption ionization time-of-flight (MALDI-TOF) mass spectrometries with appropriate ion labeling techniques (e.g., Ag^+-labeling techniques by Reinhoudt group: Timmerman, P.; Jolliffe, K. A.; Crego-Calama, M.; Weidmann, J.-L.; Prins, L. J.; Cardullo, F.; Snellink-Ruel, B. H. M.; Fokkens, R.; Nibbering, N. M. M.; Shinkai, S.; Reinhoudt, D. N. *Chem.−Eur. J.* **2000**, *6*, 4104−4115) all resulted in failure. These results strongly suggest the poor ionization property of the fully assembled *EE*-**M2**$_3$·**B2**$_3$ covered by an external aliphatic shell (see the section of NMR studies). Furthermore, we found that the mass peaks of the monomeric components in these measurements were very weak despite the fact that individual measurements of each component provided a prominent peak of the corresponding monomeric species. This is probably due to the high stability of *EE*-**M2**$_3$·**B2**$_3$, thus inhibiting the detection of the monomeric species.

timation in PS-based calibration is not surprising because the SEC retention time reflects the hydrodynamic volume of analytes and not their molecular weight.[24]

Dynamic Light Scattering Studies. To further establish the formation of rosette *EE*-**M2**$_3$·**B2**$_3$, DLS studies were carried out. For *EE*-**M2** in $CHCl_3$ (5 mM), very large aggregates with an average size that exceeds 500 nm were constantly observed. This implies that *EE*-**M2** exists in a weakly interacted assembly pool that is most likely reverse micellar-type aggregates as reported by Würthner et al.[25] Upon the addition of 1 equiv of **B2**, such large assemblies were no longer observed, indicating preferential complexation between *EE*-**M2** and **B2**. Instead, an aggregate with the hydrodynamic radius (R_h) of 4.2 nm was observed. This value corresponds well with the calculated R_h (4.8 nm) for *EE*-**M2**$_3$·**B2**$_3$ based on molecular modeling (vide infra), thus supporting the formation of a rosette between *EE*-**M2** and **B2**.

^{1}H NMR Studies. Figure 3a shows the result of the ^{1}H NMR titration experiment of *EE*-**M2** (5 mM) with **B2** in $CDCl_3$ at room temperature. Upon the addition of **B2**, new signals grew in the low-field region (signals *k**, *l**, and *b**). These resonances at $\delta = 14.1$, 13.7, and 10.4 ppm are assignable to the hydrogen-bonded H_k and H_l of **B2**, and H_b of *EE*-**M2**, respectively. In related studies, the presence of these low-field shifted signals are the best diagnostic evidence for the formation of the rosette.[26] A NOESY spectrum recorded for the 1:1 solution displayed strong intermolecular cross-peaks from H_b to both H_k and H_l, confirming the formation of the DAD·ADA hydrogen bond (Figure 3b).

Upon complexation, the signals of the azobenzene protons (H_c−H_f) and benzyl protons (H_g) of *EE*-**M2** and the olefinic (H_m), aromatic (H_n), and ether CH_2 protons (H_o and H_p) of **B2** were all heavily broadened. The degree of broadening is concentration-independent (100−2.5 mM), indicating that the observed line broadening is a consequence of the formation of a discrete cyclic assembly (rosette), the internal sites of which are poorly solvated, rigid, and highly anisotropic. Interestingly, when the amounts of *EE*-**M2** and **B2** are not equal, the signals of the excess free components (signals *c*−*g* of *EE*-**M2** when [*EE*-**M2**] < [**B2**] or signals *m*−*p* of **B2** when [*EE*-**M2**] < [**B2**])[27] are clearly discernible from the ill-defined resonances of the rosette. This finding indicates that the monomer-aggregate exchange is slow on the NMR time scale. The slow monomer-aggregate exchange is in sharp contrast to other rosette[21] or acyclic assemblies[28] lacking any covalent preorganizations, in which the NMR titration experiments conducted at room temperature only allow the observation of the averaged signals of both the monomer and the aggregate. The result of the ^{1}H NMR titration experiment of *EE*-**M2** with **B2** presented here is very reminiscent of those observed for the covalently preorganized (multi)rosette systems[22i,j,29] and provides unequivocal evidence for the formation of the thermodynamically stable rosette *EE*-**M2**$_3$·**B2**$_3$ without any covalent preorganizations.

A closer inspection reveals that the signals of the aromatic (H_h) and the ether CH_2 protons (H_i and H_j) of *EE*-**M2** remain sharp in the assembly (signals *h**, *i**, and *j**). This indicates

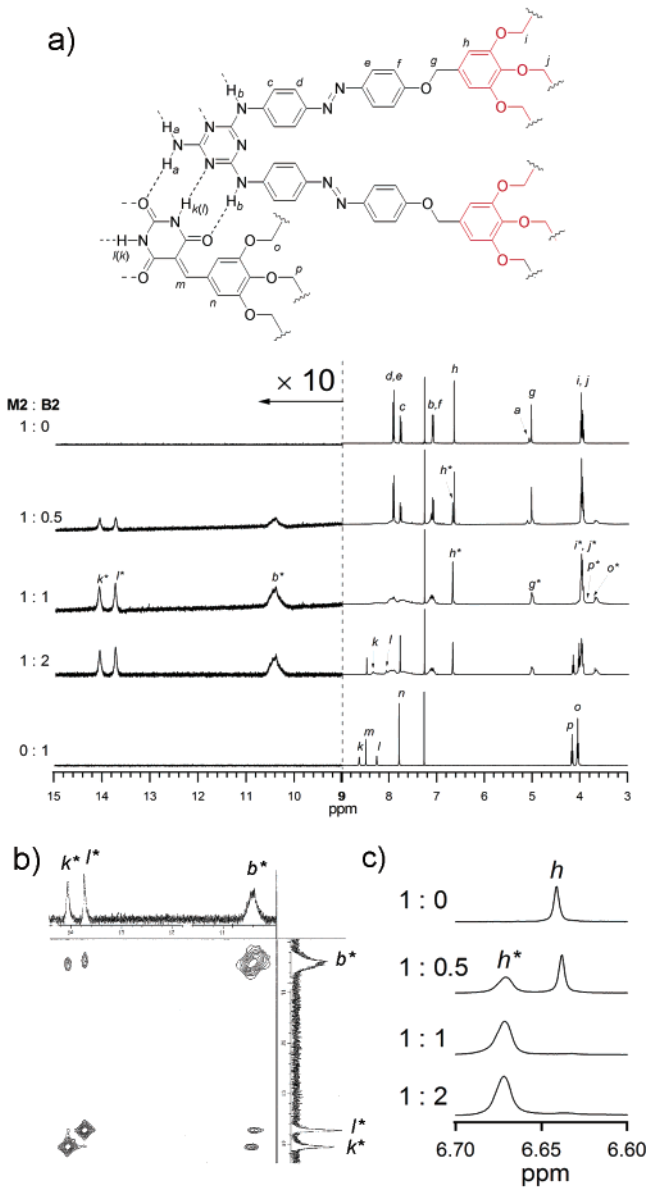

Figure 3. (a) Selected spectra for the ^{1}H NMR titration experiment of *EE*-**M2** (5 mM) with **B2** in $CDCl_3$ at room temperature. The spectrum at the bottom is that of **B2** alone (10 mM). The signals of the complexed *EE*-**M2** and **B2** are distinguished by attaching a star to the annotations. (b) A portion of the NOESY spectrum recorded at a 1:1 ratio. (c) Expanded spectra of (a) for the resonance of the aromatic protons of the TDP wedges.

(21) Mathias, J. P.; Simanek, E. E.; Zerkowski, J. A.; Seto, C. T.; Whitesides, G. M. *J. Am. Chem. Soc.* **1994**, *116*, 4316−4325.
(22) (a) Zeng, F.; Zimmerman, S. C.; Kolotuchin, S. V.; Reichert, D. E. C.; Ma, Y. *Tetrahedron* **2002**, *58*, 825−843. (b) Suárez, M.; Lehn, J.-M.; Zimmerman, S. C.; Skoulios, A.; Heinrich, B. *J. Am. Chem. Soc.* **1998**, *120*, 9526−9532. (c) Castellano, R. K.; Rebek, J., Jr. *J. Am. Chem. Soc.* **1998**, *120*, 3657−3663. (d) Zimmerman, S. C.; Zeng, F.; Reichert, D. E. C.; Kolotuchin, S. V. *Science* **1996**, *271*, 1095−1098. (e) Mathias, J. P.; Simanek, E. E.; Whitesides, G. M. *J. Am. Chem. Soc.* **1994**, *116*, 4326−4340. (f) Mathias, J. P.; Seto, C. T.; Simanek, E. E.; Whitesides, G. M. *J. Am. Chem. Soc.* **1994**, *116*, 1725−1736. (g) Yang, J.; Fan, E.; Geib, S. J.; Hamilton, A. D. *J. Am. Chem. Soc.* **1993**, *115*, 5314−5315. (h) Seto, C. T.; Whitesides, G. M. *J. Am. Chem. Soc.* **1993**, *115*, 1330−1340. (i) Seto, C. T.; Mathias, J. P.; Whitesides, G. M. *J. Am. Chem. Soc.* **1993**, *115*, 1321−1329. (j) Seto, C. T.; Whitesides, G. M. *J. Am. Chem. Soc.* **1993**, *115*, 905−916.
(23) The rosette composed of TDP-lacking **M1** and **B1** did not elute from the SEC column because it decomposed during the analysis and the resulting components were adsorbed to the column matrix.
(24) Similar overestimations have been reported in the SEC analyses of structurally related azobenzene-containing dendrons possessing a large number of long alkyl chains: (a) Yokoyama, S.; Nakahama, T.; Otomo, A.; Mashiko, S. *J. Am. Chem. Soc.* **2000**, *122*, 3174−4181. (b) Percec, V.; Cho, W.-D.; Ungar, G. *J. Am. Chem. Soc.* **2000**, *122*, 10273−10281.
(25) Thalacker, C.; Würthner, F. *Adv. Funct. Mater.* **2002**, *12*, 209−218.
(26) (a) Simanek, E. E.; Wazeer, M. I. M.; Mathias, J. P.; Whitesides, G. M. *J. Org. Chem.* **1994**, *59*, 4904−4909. (b) Chin, D. N.; Simanek, E. E.; Li, X.; Wazeer, M. I. M.; Whitesides, G. M. *J. Org. Chem.* **1997**, *62*, 1891−1895. (c) Prins, L. J.; Jolliffe, K. A.; Hulst, R.; Timmerman, P.; Reinhoudt, D. N. *J. Am. Chem. Soc.* **2000**, *122*, 3617−3627.

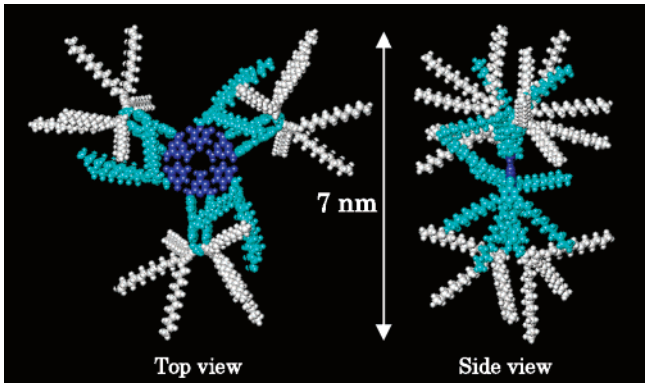

Figure 4. CPK molecular model of energy-minimized rosette *EE*-**M2**$_3$·**B2**$_3$.

that the two TDP wedges (red colored in Figure 3a) in the complexed *EE*-**M2** can gyrate around the $C_{benzyl}-C_{ipso}$ bond and are well-solvated. Such structural features are well-illustrated by the CPK molecular models of the energy-minimized rosette *EE*-**M2**$_3$·**B2**$_3$ (Figure 4). The structure of *EE*-**M2**$_3$·**B2**$_3$ is composed of (i) a internal melamine−barbiturate hydrogen-bonded network (blue), which is surrounded by (ii) a rigid middle tier involving the azobenzene moieties of *EE*-**M2** and the TDP wedges of **B2** (cyan), which is further surrounded by (iii) external conformationally free TDP wedges of *EE*-**M2** (white). Such an architecture is considered to stabilize the assembly because the exterior aliphatic chains effectively protect the hydrogen-bonded core from solvation. It should be noted that the rigid *E*-azobenzene moieties in *EE*-**M2** separate the bulky TDP wedges from the triazine hydrogen-bonding functionality, providing a suitable *EE*-**M2**·**B2** alternate arrangement in the rosette architecture by decreasing the steric interactions between the TDP wedges of *EE*-**M2** and **B2**.[30−32]

To shed light on the stability of rosette *EE*-**M2**$_3$·**B2**$_3$, a DMSO-d_6 titration experiment was performed.[33] The titration of *EE*-**M2**$_3$·**B2**$_3$ (5 mM in $CDCl_3$) with hydrogen-bond breaking DMSO-d_6 resulted in the decomposition of *EE*-**M2**$_3$·**B2**$_3$ into monomers without any intermediate species. *EE*-**M2**$_3$·**B2**$_3$ was completely decomposed in 21% (v/v) DMSO-d_6/$CDCl_3$, far more stable than the previously reported TDP-lacking rosette **M1**$_3$·**B1**$_3$[12] that completely decomposed only in 3% (v/v) DMSO-d_6/$CDCl_3$. Moreover, the stability of *EE*-**M2**$_3$·**B2**$_3$ in the DMSO-d_6 titration experiment was comparable to those of the covalently preorganized rosettes[29,33,34] as well as the self-assembling dendrimers[16] based on robust DDA·AAD-type hydrogen bonding. The stability of *EE*-**M2**$_3$·**B2**$_3$ might be further highlighted in the presence of polar DMSO molecules by the solvophobic effect of the TDP wedges.

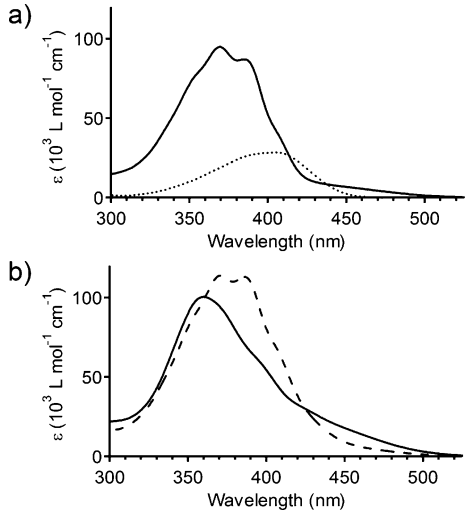

Figure 5. (a) UV−vis spectra of *EE*-**M2** (solid line) and **B2** (dotted line) in MCH (10 μM). (b) Solid line: UV−vis spectrum of the equimolar mixture of *EE*-**M2** (10 μM) and **B2** (10 μM) in MCH. Dashed line: the sum of the two spectra in (a).

Rosette *EE*-**M2**$_3$·**B2**$_3$ in $CDCl_3$ was stable for more than one month as monitored by ^{1}H NMR. Neither the precipitation of the competing tapelike assemblies often observed in the other rosettes that lack the covalent preorganization[12,34b] nor the hierarchical association of the rosette[18a,b,35] was observed even at very high concentrations (100 mM), as confirmed by ^{1}H NMR. The latter supports the nondisklike morphology of the rosette with the freely gyrable six TDP wedges of *EE*-**M2** (Figure 4), which is unfavorable for further stacking in solution. Thus, the rosette *EE*-**M2**$_3$·**B2**$_3$ is the thermodynamic product.

UV−Vis Studies. Aggregation between *EE*-**M2** and **B2** in MCH was studied by UV−vis spectroscopy.[22i,j,36,37] Making use of the least polar solvents such as methylcyclohexane (MCH) promises strong binding events between polar functionalities, shifting the equilibrium toward aggregates even under highly diluted conditions.[38] Figure 5a shows the UV−vis spectra of the individual components, *EE*-**M2** (solid line) and **B2** (dotted line), in MCH. Melamine *EE*-**M2** shows a structured absorption band with λ_{max} at 370 and 380 nm, which is attributed to the

(27) Because of the self-aggregation property of **B2**, the signals of the imide protons (signals *k* and *l*) of the residual **B2** shifted to low field with its increasing concentration.
(28) Würthner, F.; Thalacker, C. Sautter, A. *Adv. Mater.* **1999**, *11*, 754−758.
(29) (a) Vreekamp, R. H.; van Duynhoven, J. P. M.; Hubert, M.; Verboom, W.; Reinhoudt, D. N. *Angew. Chem., Int. Ed. Engl.* **1996**, *35*, 1215−1218. (b) Timmerman, P.; Vreekamp, R. H.; Hulst, R.; Verboom, W.; Reinhoudt, D. N.; Rissanen, K.; Udachin, K. A.; Ripmeester, J. *Chem.−Eur. J.* **1997**, *3*, 1823−1832.
(30) Zimmerman (ref 16), Reinhoudt, and Fréchet independently reported the supramolecular dendrimers composed of six hydrogen-bonding dendrons: (a) Huck, W. T. S.; Hulst, R.; Timmerman, P.; van Veggel, F. C. J. M.; Reinhoudt, D. N. *Angew. Chem., Int. Ed. Engl.* **1997**, *36*, 1006−1008. (b) Freeman, A. W.; Vreekamp, R. H.; Fréchet, J. M. J. *Polym. Mater. Sci. Eng.* **1997**, *77*, 138−139. In the former two systems, an increase in the generation of dendrons resulted in a decrease in the stability of the self-assembling dendrimers by gaining a steric interaction between them.
(31) Würthner et al. reported the liquid-crystalline bulk materials composed of coaggregates of TDP-attached melamine and merocyanine-type barbiturate, both structurally related to **M2** and **B2**, respectively: Würthner, F.; Yao, S.; Heise, B.; Tschierske, C. *Chem. Commun.* **2001**, 2260−2261. In this case, a linear tapelike assembly was deduced from the XPD studies.
(32) One of the reviewers suggested that the present rosette can be called "monodisperse inverse micelles" when taking into account that the exterior alkyl chains are not stretched in an all-transoid conformation.
(33) Mammen, M.; Simanek, E. E.; Whitesides, G. M. *J. Am. Chem. Soc.* **1996**, *118*, 12614−12623.
(34) The association constant for the melamine−barbiturate complexation has proved to be 2 orders of magnitude lower than that for the melamine−cyanurate complexation: (a) Prins, L. J.; Verhage, J. J.; de Jong, F.; Timmerman, P.; Reinhoudt, D. N. *Chem.−Eur. J.* **2002**, *8*, 2302−2313. (b) Bielejewska, A. G.; Marjo, C. E.; Prins, L. J.; Timmerman, P.; de Jong, F.; Reinhoudt, D. N. *J. Am. Chem. Soc.* **2001**, *123*, 7518−7533. Taking into account the lower binding strength of the melamine−barbiturate system, the stability of **M2**$_3$·**B2**$_3$ should be further emphasized when compared with the Whitesides and Reinhoudt's double rosette based on the melamine−cyanurate complexation.
(35) (a) Yang, W.; Chai, X.; Chi, L.; Liu, X.; Cao, Y.; Lu, R.; Jiang, Y.; Tang, X.; Fuchs, H.; Li, T. *Chem.−Eur. J.* **1999**, *5*, 1144−1149. (b) Kimizuka, N.; Kawasaki, T.; Hirata, K.; Kunitake, T. *J. Am. Chem. Soc.* **1995**, *117*, 6360−6361. (c) Kimizuka, N.; Fujikawa, S.; Kuwahara, H.; Kunitake, T.; Marsh, A.; Lehn, J.-M. *J. Chem. Soc., Chem. Commun.* **1995**, 2103−2104.
(36) Prins, L. J.; Thalacker, C.; Würthner, F.; Timmerman, P.; Reinhoudt, D. N. *Proc. Natl. Acad. Sci. U.S.A.* **2001**, *98*, 10042−10045.
(37) Drain, C. M.; Russell, K. C.; Lehn, J.-M. *Chem. Commun.* **1996**, 337−338.
(38) Würthner, F.; Thalacker, C.; Sautter, A.; Schärtl, W.; Ibach, W.; Hollricher, O. *Chem.−Eur. J.* **2000**, *6*, 3871−3886.

$\pi-\pi^*$ transition moment along the long axis of the azobenzene chromophores. This band is almost superimposable on that of the molecularly dissolved 4-amino-4′-tri(dodecyloxy)phenoxyazobenzene in MCH, indicating that *EE*-**M2** exists in the molecularly dissolved state in MCH at this concentration (10 μM). Chromogenic barbituric acid **B2** has an absorption band at $\lambda_{max} = 405$ nm, which is assignable to the intramolecular CT transition.

The UV−vis spectrum of an equimolar mixture of *EE*-**M2** (10 μM) and **B2** (10 μM) in MCH (solid line in Figure 5b) showed clear aggregation-induced changes when compared with the summed spectrum of those of the individual components (dashed line in Figure 5b). The $\pi-\pi^*$ absorption band of the azobenzene chromophore hypsochromically shifts by 10 nm (750 cm^{-1}) and becomes less structured with a single λ_{max} at 360 nm.[39] A Job's plot using the hypsochromic shift as a probe confirmed the 1:1 complexation between *EE*-**M2** and **B2** (data not shown). Decreasing the concentration ($10^{-3} \rightarrow 10^{-8}$ M) or increasing the temperature (20 → 90 °C) resulted in the spectral changes corresponding to the aggregate-to-monomer transition in relatively narrow concentration ($10^{-5} \rightarrow 10^{-8}$ M) and temperature ranges (40 → 70 °C),[40] reconciled with the cooperative dissociation of the discrete cyclic assembly *EE*-**M2**$_3$·**B2**$_3$ (see Supporting Information). The hypsochromic shift is assignable to the strong intramolecular electronic interaction between the two azobenzene moieties of *EE*-**M2**, the conformations of which are fixed to syn upon complexation with **B2**.[39] In addition to the hypsochromic shift of the $\pi-\pi^*$ absorption band of the azobenzene chromophores of *EE*-**M2**, the absorption intensity is increased around 450 nm. The UV−vis analysis of **B2** upon binding with *N*,*N*′-di(*p*-*tert*-butylphenyl)melamine, transparent in the visible region, revealed that this change comes from the complexation-induced spectral broadening of **B2**.

Photoisomerization Studies. With the prima facie evidence for the formation of the stable rosette *EE*-**M2**$_3$·**B2**$_3$ in hand, we next investigated the photoresponsive property of the assembly. Figure 6a shows the UV−vis absorption spectral change of *EE*-**M2** (10 μM) in MCH upon irradiation at around 380 nm. The azobenzene moieties of the molecularly dissolved *EE*-**M2** showed facile $E \rightarrow Z$ isomerization as demonstrated by the decrease in the $\pi-\pi^*$ absorption band of the *E*-isomer that peaked at 370 nm with a concomitant increase in the $\pi-\pi^*$ and $n-\pi^*$ bands of the *Z*-isomer that peaked at 318 and 452 nm, respectively. A photostationary state was attained within 20 min at which the *E*/*Z* ratio was 3:97 from the decrease in the absorption intensity at 370 nm. The facile isomerization indicates the efficient conversion from *EE*-**M2** into *ZZ*-**M2**. The *Z*-azobenzene moieties of *ZZ*-**M2** can be photochemically reconverted to the *E*-isomer by irradiating at around 450 nm for 30 min (*E*/*Z* = 85:15) or thermally by storage in the dark at 25 °C for 12 h (*E*/*Z* = 99:1, $t_{1/2} = 4$ h).

In sharp contrast, when an equimolar mixture of *EE*-**M2** and **B2** in MCH (10 μM) was irradiated at around 380 nm for more than 1 h, the decrease in the $\pi-\pi^*$ absorption band was only ca. 30% (Figure 6b), indicating the suppression of the $E \rightarrow Z$ isomerization of the azobenzene moieties in the rosette.[4b,8i]

(39) An analogous small hypsochromic shift has been reported for dimeric methyl red dyes attached to a single-stranded DNA: Asanuma, H.; Shirasuka, K.; Takarada, T.; Kashida, H.; Komiyama, M. *J. Am. Chem. Soc.* **2003**, *125*, 2217−2223.

(40) For details, see Supporting Information.

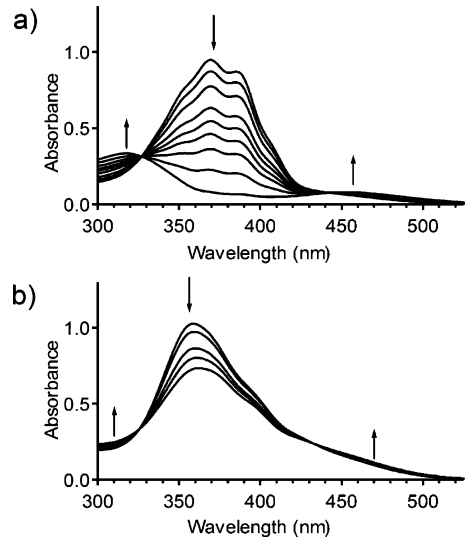

Figure 6. UV−vis spectral changes of *EE*-**M2** (10 μM) in MCH upon irradiation at around 380 nm (a) for 20 min in the absence of **B2** and (b) for 1 h in the presence of 1 equiv of **B2**.

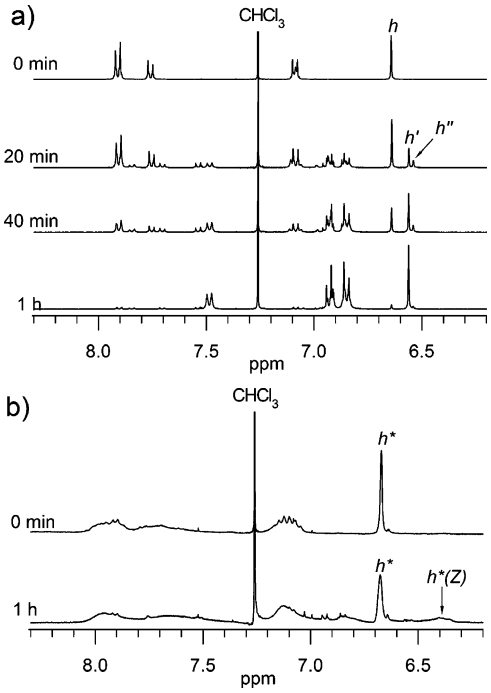

Figure 7. ^{1}H NMR spectral changes of *EE*-**M2** (5 mM) in $CDCl_3$ upon irradiation at around 380 nm for 1 h (a) in the absence and (b) in the presence of 1 equiv of **B2**.

Suppression of the photoisomerization was not observed when monotopic **B3** was used as a partner for **M2**. Obviously, the suppression is caused by complexing with the ditopic **B2**, i.e., this is a unique property induced by the formation of the rosette. The degree of suppression is constant at the concentration of the assembly ranging from 10^{-3} to 10^{-5} M, at which the quantitative formation of the assembly had been confirmed by the UV−vis dilution experiments (see Supporting Information).

The $E \rightarrow Z$ photoisomerization experiments were also carried out in $CDCl_3$ by monitoring using ^{1}H NMR spectroscopy. Figure 7a shows the ^{1}H NMR spectral changes of *EE*-**M2** in $CDCl_3$ upon irradiation at around 380 nm. The three discrete isomers, i.e., *EE*-**M2**, *EZ*-**M2**, and *ZZ*-**M2**, were clearly distinguishable in the ^{1}H NMR spectra, especially by the aromatic proton signals

of the TDP wedges (signal *h*). For the irradiation period of 20 min, two additional signals emerged at $\delta = 6.56$ (signal *h*′) and 6.53 ppm (signal *h*″). Further irradiation (40 min) resulted in an increase in the intensity of the signal *h*′ in compensation for a decrease in the intensity of the signal *h* of *EE*-**M2**, and finally, the signal *h*′ became predominant after irradiation for 1 h. Simultaneous UV−vis measurements ensured that the predominant signal *h*′ is derived from *ZZ*-**M2**. Thus, the signal *h*″, which remained small for any irradiation time, is assignable to the aromatic protons of the TDP wedge attached to the *Z*-azobenzene moiety of the intermediate isomer *EZ*-**M2**. Analysis of the integrations of these three signals (*h*, *h*′, and *h*″) revealed that the aromatic protons of the TDP wedge attached to the *E*-azobenzene moiety of *EZ*-**M2** overlap with the signal *h* of *EE*-**M2**. A photostationary state was attained by the 1-h irradiation, giving the *E*/*Z* ratio of 4:96 (*EE*-**M2**/*EZ*-**M2**/*ZZ*-**M2** = 0:8:92).[41]

The $E \rightarrow Z$ photoisomerization of the azobenzene moiety of *EE*-**M2** was also suppressed in $CDCl_3$ by complexing with **B2**. Figure 7b shows the ^{1}H NMR spectral changes of the 1:1 mixture of *EE*-**M2** and **B2** in $CDCl_3$ (5 mM) by irradiation at around 380 nm for 1 h (photostationary state). Because of their ill-defined resonances, no notable change was found in the protons of the azobenzene moiety ($\delta = 6.8-8.1$ ppm). A pronounced change was found in the aromatic protons of the TDP wedges of **M2**, which had proven to be a good indicator for complexation with **B2** in the NMR titration experiment (see Figure 3c). A new highly broadened resonance (*h**(*Z*)) emerged alongside the sharp signals of the aromatic protons of the TDP wedges attached to the *E*-azobenzene moiety in the rosette (*h**). This resonance is assignable to the signals of the aromatic protons of the TDP wedge attached to the *Z*-azobenzene moiety in the rosette. The broadening indicates that the TDP wedge attached to the *Z*-azobenzene moiety cannot gyrate in the rosette, very likely because of the steric interaction with the TDP wedge of the adjacent **B2** molecules. The *E*/*Z* ratio could be determined as 74:26 by the integration of the signals after decomposition of the assembly by adding DMSO-d_6. This ratio is consistent with that for the rosette in MCH estimated by UV−vis spectroscopy (see Figure 6b). The *E*/*Z* ratio of roughly 7:3 indicates that two of the six azobenzene moieties in a rosette can undergo $E \rightarrow Z$ isomerization.

McGrath et al. have extensively investigated the effect of the *E*/*Z* isomerization of azobenzene-appended dendrimers on their hydrodynamic volumes by SEC analysis.[9a,f,42] For the benzyl aryl ether dendrimers possessing three or six azobenzene moieties at the core, which is structurally related to our rosette, their SEC retention times could be moderately modulated (hydrodynamic volumes changed by 16−29%) by dark incubation and extensive UV-light irradiation.[42] As expected, the UV-irradiation of *EE*-$\mathbf{M2}_3$·$\mathbf{B2}_3$ induced no changes in its SEC retention time because of the low photoisomerization yield in the rosette.

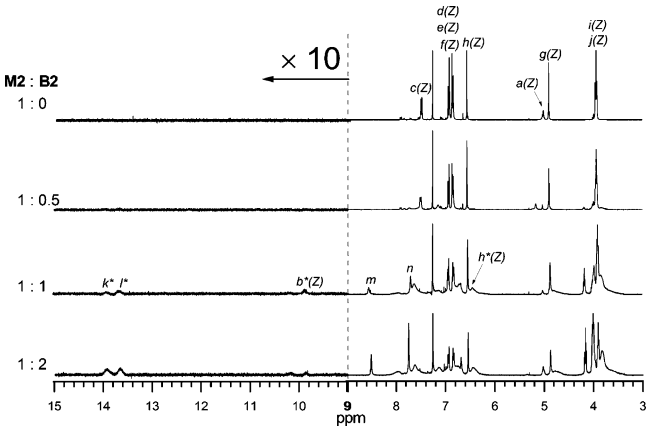

Figure 8. Selected spectra for the ^{1}H NMR titration experiment of preliminary UV-irradiated **M2** (5 mM, *EE*-**M2**/*EZ*-**M2**/*ZZ*-**M2** = 0:8:92) with **B2** in $CDCl_3$. Annotations refer to Figure 3.

In the previously reported rosette $\mathbf{M1}_3$·$\mathbf{B1}_3$, 88% of the *E*-azobenzene moiety photoisomerized into the *Z*-isomer.[12] From the structural difference in the supramolecular synthons, it is apparent that the suppression of the photoisomerization of the azobenzene moieties in *EE*-$\mathbf{M2}_3$·$\mathbf{B2}_3$ stems from the presence of the bulky TDP wedges. This implies a structural incompatibility between *ZZ*-**M2** and the rosette architecture, and it prompted us to investigate the aggregation behavior of the initially photogenerated *ZZ*-**M2** with **B2**.

The complexation behavior of *ZZ*-**M2** with **B2** was studied by ^{1}H NMR titration of the initially UV-irradiated **M2** (*EE*-**M2**/*EZ*-**M2**/*ZZ*-**M2** = 0:8:92) with **B2** (Figure 8). Upon the addition of **B2**, three resonances (signals *k**, *l**, and *b**(*Z*)), diagnostic for the rosette, emerged at $\delta = 13.9$, 13.6, and 9.9 ppm, respectively. These three signals are slightly high-field shifted in comparison with those of the rosette *EE*-$\mathbf{M2}_3$·$\mathbf{B2}_3$ ($\delta = 14.1$, 13.7, and 10.4 ppm, respectively). The discrepancy in these chemical shifts is an indication of the involvement of the *Z*-azobenzene moieties in the rosette. This is also supported from the growth of the signal *h**(*Z*) corresponding to the aromatic protons of the TDP wedge attached to the *Z*-azobenzene moiety in the rosette (see Figure 7b).

Interestingly, through the titration, the sharp signals of the free *ZZ*-**M2** remain dominant even in the presence of excess **B2**. This observation indicates the low complexation efficiency of *ZZ*-**M2** with **B2**. Indeed, the intensities of the signals *k**, *l**, and *b**(*Z*), diagnostic for the rosette, were unambiguously weak in comparison with the titration experiment of *EE*-**M2** (see Figure 3a). Plots of the fraction of the aggregated **M2** (α_{agg}) versus the molar ratio [**B2**]/[**M2**] in the NMR titration experiments conducted for *EE*-**M2** (Figure 3a) and *ZZ*-**M2** (Figure 8) more clearly highlight the difference between their complexation efficiency with **B2** (Figure 9). In clear contrast to the quantitative

(41) In this experiment, a small proportion of the intermediate species *EZ*-**M2** for any irradiation time strongly suggests the cooperative $E \rightarrow Z$ isomerization of the two azobenzene moieties of *EE*-**M2**; isomerization of one of the two *E*-azobenzene moieties promotes subsequent isomerization of another one: (a) Itoho, K.; Masuda, T.; Takei, M.; Sakurai, Y.; Nishigami, M. *J. Chem. Soc., Chem. Commun.* **1986**, 1028−1030. The reason for the cooperative photoisomerization is ambiguous; however, it may come from a weak electronic interaction between the two syn-arranged azobenzene moieties in a *EE*-**M2** molecule in $CDCl_3$. This is consistent with the DLS study of *EE*-**M2** in $CHCl_3$ that showed the presence of a large aggregated species. In such self-aggregates, two bulky *N*-substituents of melamine must be fixed to the syn arrangement by intermolecular hydrogen bonding (see ref 25). An alternative explanation for the weak electronic interaction could be provided by invoking a recent report by Ghiviriga et al.: (b) Ghiviriga, I.; Oniciu, D. C. *Chem. Commun.* **2002**, 2718−2719. They experimentally showed that the two bulky substituents substituted at the two amino groups of melamine preferably take the syn conformation in the solvents that can weakly coordinate to the nitrogen atoms of the triazine ring, such as $CDCl_3$, as a result of mitigation of the steric hindrance to solvation.

(42) (a) Liao, L.-X.; Junge, D. M.; McGrath, D. V. *Macromolecules* **2002**, *35*, 319−322. (b) Li, S.; McGrath, D. V. *J. Am. Chem. Soc.* **2000**, *122*, 6795−6796.

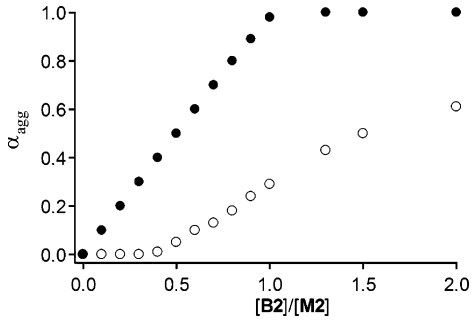

Figure 9. Plots of the fraction of aggregated **M2** (α_{agg}) versus molar ratio [**B2**]/[**M2**]. Data for *EE*-**M2** (●) and *ZZ*-**M2** (○) were taken from Figures 3a and 8, respectively.

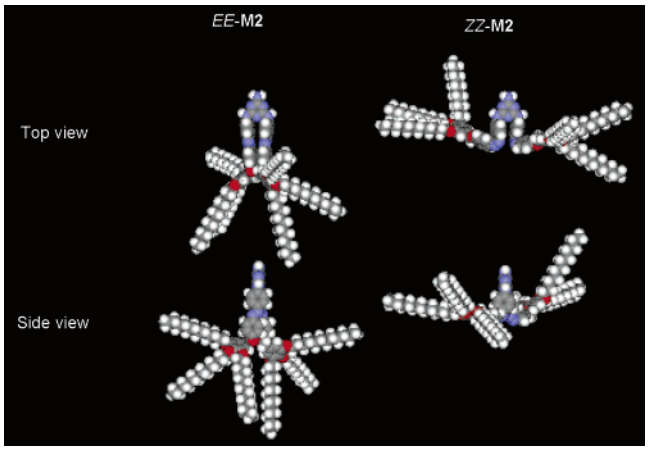

Figure 10. Energy-minimized structures of *EE*-**M2** (left) and *ZZ*-**M2** (right).

complexation of *EE*-**M2** (●), the complexation efficiency of *ZZ*-**M2** (○) is significantly low. At the 1:1 ratio, only 30% of *ZZ*-**M2** complexes with **B2** to form rosettes.[43] The observed difference can be taken as a consequence of the steric interaction between the TDP wedges of *ZZ*-**M2** and **B2** in the complexation process.

The CPK molecular models of the energy-optimized *EE*-**M2** and *ZZ*-**M2** shown in Figure 10 nicely depict the observed difference in their complexation efficiencies. In *EE*-**M2**, the *E*-azobenzene moieties separate the bulky TDP wedges from the melamine hydrogen-bonding sites, providing sufficient space for binding with **B2**. In sharp contrast, the TDP wedges of *ZZ*-**M2** project toward the hydrogen-bonding sites because of the folded conformation of the *Z*-azobenzene moieties. One can easily envision that such a molecular geometry is quite a disadvantage for binding with **B2** in the rosette motif.[44] Indeed, we could not construct rosette *ZZ*-$\mathbf{M2}_3$·$\mathbf{B2}_3$ without any intermolecular steric interactions between the TDP wedges of *ZZ*-**M2** and **B2**.

The photoregulatable complexation efficiency of **M2** finally prompted us to carry out the phototriggered formation of the rosette. Figure 11 shows the UV−vis spectral changes of the 1:1 mixture of *ZZ*-**M2** (94% isomeric purity) and **B2** (10 μM) in MCH upon irradiation at around 450 nm. The irradiation

(43) As one of the reviewers pointed out, a rosette might be formed if at least some *EZ*-**M2** molecules are involved in the rosette with *ZZ*-**M2**. In other words, *ZZ*-**M2** alone could not form a rosette with **B2**. This suggestion is fully consistent with the result of the molecular modeling study as well as the result of the phototriggered SEC experiment described below.

(44) A similar steric argument was done for the self-assembling dendrimers: see refs 16 and 30.

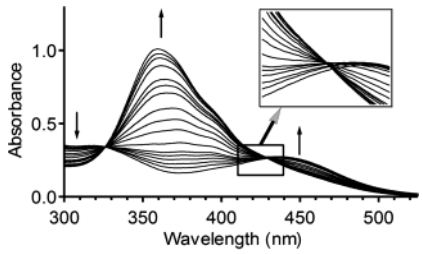

Figure 11. UV−vis spectral changes of an equimolar mixture of *ZZ*-**M2** (10 μM) and **B2** (10 μM) in MCH upon irradiation at around 450 nm for 30 min.

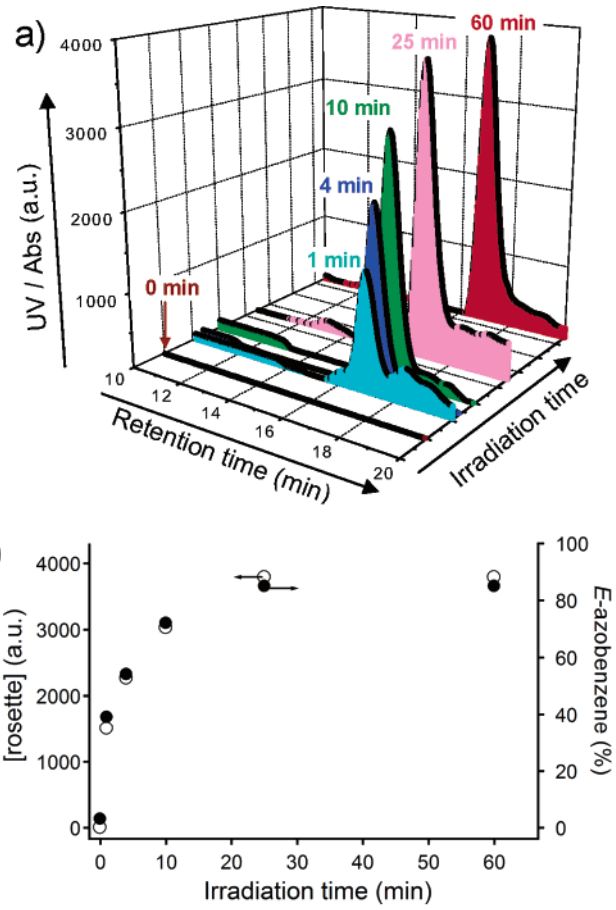

Figure 12. (a) Phototriggered formation of the rosette monitored by SEC upon irradiation of a nearly equimolar mixture of *ZZ*-**M2** (94% isomeric purity, 50 μM) and **B2** (50 μM) in toluene at around 450 nm. (b) Plots of the concentration of the rosette in the SEC analyses (○, left *Y* axis) and the mole fraction of the *E*-azobenzene moiety estimated from the simultaneous UV−vis measurements (●, right *Y* axis) versus the irradiation time of 450-nm visible light (*X* axis).

resulted in an increase in the absorption at around 370 nm and a decrease in the absorption at around 320 and 450 nm, showing $Z \rightarrow E$ isomerization of the azobenzene moiety. After irradiation for 30 min, the spectral shape was almost identical to that of the stoichiometric mixture of *EE*-**M2** and **B2** (solid line in Figure 5b), indicating that regenerated *EE*-**M2** formed a rosette with **B2**. During the course of the $Z \rightarrow E$ isomerization, a clear isosbestic point was observed in the shorter wavelength region at around 325 nm where absorption of **B2** is weak, whereas no isosbestic point was observed in the longer wavelength region at around 430 nm (inset) where the absorption of **B2** significantly overlaps. This finding implies that the $Z \rightarrow E$ isomerization of the azobenzene moiety of **M2** is accompanied by the

Scheme 1. Schematic Representation of the Aggregation of **M2** (red) and **B2** (blue) with the Photoresponsive Properties Therein

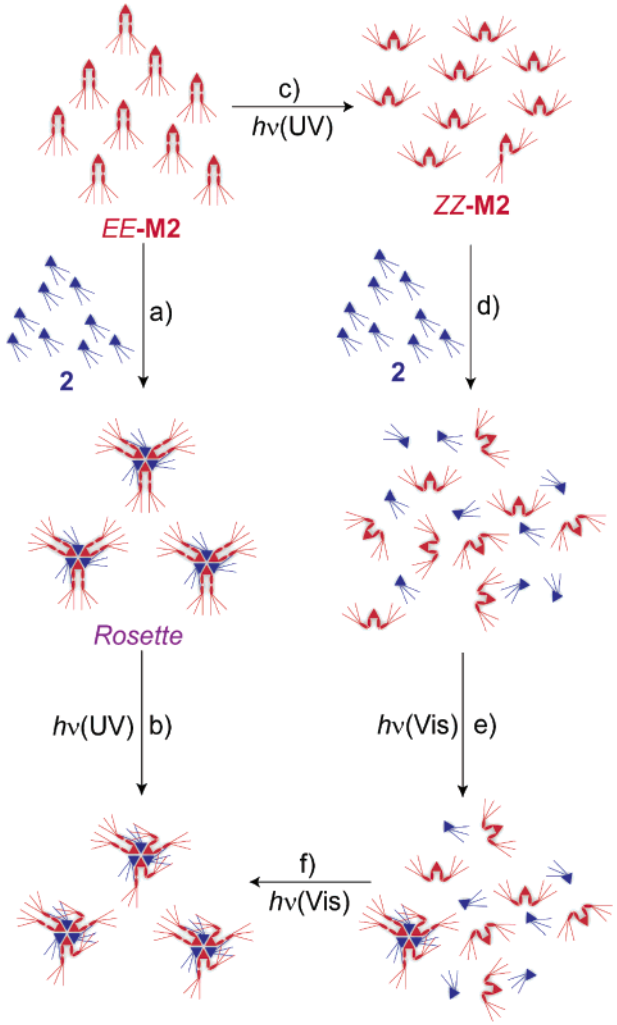

absorption spectral change of **B2**. Since the chromogenic barbiturate **B2** has been shown to exhibit aggregation-induced absorption spectral changes (vide supra), this result demonstrates that the $Z \rightarrow E$ isomerization of the azobenzene moiety triggers the complexation of **M2** with **B2**.

The phototriggered formation of the rosette was demonstrated more strikingly, yet impressively by the SEC analysis. Figure 12a shows the change in the SEC trace of an equimolar mixture of *ZZ*-**M2** (ca. 94% isomeric purity) and **B2** in toluene upon irradiation at around 450 nm for 60 min. The concentrations of the components were 50 μM, at which no aggregated species were detected in the ^{1}H NMR spectrum in toluene-d_8. The UV detection wavelength for the SEC analysis was set to 325 nm, an isosbestic point in the UV−vis spectral change of the $Z \rightarrow E$ isomerization (Figure 11). Detection at this wavelength allows the SEC analysis regardless of the absorption spectral difference between the *Z*- and *E*-azobenzene moieties. Before irradiation at around 450 nm (brown trace in Figure 12a), no prominent peak was observed, indicating the absence of the rosette with detectable concentration. This condition could be retained when the solution was continuously irradiated with UV light or incubated at 0 °C in the dark. Notably, irradiation at around 450 nm resulted in an increase in the SEC peak corresponding to the rosette (1−25 min in Figure 12a). Figure 12b shows the plots of the SEC peak intensity of the rosette (○) and the mole fraction of the *E*-azobenzene moiety (●, estimated from simultaneous UV−vis measurements) versus the irradiation time. The increase in the rosette concentration corresponds to the increase in the mole fraction of the *E*-azobenzene moiety. After irradiation for 25 min, the increase in the rosette concentration leveled off, concomitantly with the photostationary state obtained in the simultaneous UV−vis measurements. By taking into account that the construction of the hydrogen-bonded assembly is a rapid process, it is evident that the $Z \rightarrow E$ isomerization of the azobenzene moiety regulates the formation of the rosette.

Taken together, the overall self-assembly process between **M2** and **B2** with the phototriggered formation of the rosette can be schematically drawn as Scheme 1: (a) Melamine **M2** possessing two *E*-azobenzene moieties (*EE*-**M2**) complexes with **B2** to form the thermodynamically stable rosette *EE*-**M2**$_3$·**B2**$_3$. (b) UV-light irradiation of **M2** alone leads to the efficient $E \rightarrow Z$ photoisomerization of the azobenzene moiety to give *ZZ*-**M2**, whereas (c) that of rosette *EE*-**M2**$_3$·**B2**$_3$ results in a low yield of the $E \rightarrow Z$ photoisomerization. (d) It is hard for the photogenerated *ZZ*-**M2** to form a rosette with **B2**. (e and f) Visible-light irradiation of the monomeric mixture of *ZZ*-**M2** and **B2** triggers the formation of the rosette.

Conclusion

The combination of the two supramolecular synthons, the melamine−azobenzene−TDP conjugate **M2** and the barbituric acid−TDP conjugate **B2**, provided a hydrogen bond-directed cyclic hexamer (rosette) with high stability and photoresponsibility. The stability of the present assembly is remarkable when compared to a similar class of hydrogen-bonded cyclic assemblies. The strategy for stabilizing the supramolecular assembly presented here can be readily accomplished by simple modulation of the supramolecular synthons, and therefore, it is useful to obtain a stable noncovalently organized edifice.

Because of the large structural change of *EE*-**M2** into *ZZ*-**M2** accompanying the $E \rightarrow Z$ isomerization of the photoresponsive moiety, a clear decrease in complexation efficiency was observed between *ZZ*-**M2** and **B2**. The photoregulatable complexation ability of **M2** with **B2** leads to the successful phototriggered formation of the rosette by irradiating the simple mixture of *ZZ*-**M2** and **B2** with visible light. Thus, the formation of the well-defined nanoscale object has been regulated by a convenient external stimulus, light. Application of the present strategy to other supramolecular assemblies with the desired function may realize smart nanomaterials that can output such functions at any time on demand.

Acknowledgment. We thank Prof. Dr. Keiko Nishikawa (Chiba University) for technical assistance with the DLS measurements, Prof. Dr. Kentaro Yamaguchi and Dr. Yoshihisa Sei (Chiba University) for the CSI- and ESI-MS measurements, and Prof. Dr. Hitoshi Tamiaki and Mr. Michio Kunieda (Ritsumeikan University) for measurement of the NOESY spectra and molecular modeling calculations. We thank the reviewers for their fruitful comments on our manuscript.

Supporting Information Available: Experimental details. This material is available free of charge via the Internet at http://pubs.acs.org.

JA047783Z